

Efficient Extension to Quadrilateral Element of Three Field Hu-Washizu 2D Elasticity Formulation Based on Biorthogonal Systems

B.P. Lamichhane¹, M.Pingaro^{2,*}, P.Venini^{2,*}

Abstract

New quadrilateral mixed finite element based on modified Hu-Washizu formulation are presented. Hu-Washizu is a three field formulation where the unknowns are: displacement, stress and strain. The stability and consistency of the element are obtained by adding different types of bubble functions at the displacement field. Different types of bubble functions are successfully investigated and analyzed. In order to obtain an efficient discretization scheme, we use a pair of finite element bases forming a biorthogonal system between strain and stress. The biorthogonality relation allows us to statically condense out the strain and stress from the saddle-point system leading to a symmetric and positive-definite system. The strain and stress can be recovered in a post-processing step simply by inverting a diagonal matrix. Numerical examples prove the efficiency and the stability of the elements in the case of incompressible limit and distorted meshes.

Keywords: mixed finite elements, quadrilateral element, Hu-Washizu, biorthogonal systems, elasticity.

*Corresponding author.

Email addresses: Bishnu.Lamichhane@newcastle.edu.au (B.P. Lamichhane), marco.pingaro@iusspavia.it (M.Pingaro), paolo.venini@unipv.it (P.Venini)

¹School of Mathematical and Physical Sciences, University of Newcastle, Callaghan, NSW 2308

²Department of Civil Engineering and Architecture, University of Pavia, Pavia, Italy

1. Introduction

In the linear and non-linear elasticity when the Lamé constant λ tends to infinity the standard finite element exhibit some problems of convergence as locking phenomena. In this context mixed formulations are used effectively to solve this inconvenient. One of the most popular mixed formulation adopted is the Hellinger-Reissner formulation, which one describe the problem adopting as variables the stresses and the displacements. This type of formulation requires the fulfillment of the inf-sup condition as described in D.Boffi et al. (2013). Employing the Hellinger-Reissner formulation many elements have been created such as D.N.Arnold and R.Winther (2002) for triangle elements and D.N.Arnold and G.Awanou (2005) for quadrilateral. Another type of mixed formulation is the Hu-Washizu formulation (see H.Hu (1955); K.Washizu (1982)) that it is a three-field formulation introduced by B.M.Fraeijns de Veubeke (1951). One examples of Hu-Washizu formulation applied at linear and non-linear elasticity using quadrilaterals and hexahedra are reported in E.P. Kasper and R.L. Taylor (2000). In B.P.Lamichhane et al. (2006) are showed that the modify Hu-Washizu formulation are able to obtaining uniform convergence of the finite element approximation in the nearly incompressible regime in the case of quadrilateral elements. The goal of this work is to present an extension of the modified three-field formulation Hu-Washizu presented in B.P.Lamichhane (2009) using the quadrilateral elements. In accordance to B.P.Lamichhane et al. (2013) we adopt the idea to create a biorthogonal system between the stresses and strains. This assumption is essentially for the static condensation of the stresses and strains for obtain a linear system in the only unknown displacement field. In order to ensure the stability of the element we enrich the space of displacement field with different type of bubble functions in accordance to W.Bai (1997); B.P.Lamichhane (2015) for the Stokes problem. In W.Bai (1997) we adopt two bubble functions to stabilize the element, while in B.P.Lamichhane (2015) use one single bubble function are adopted.

The structure of the paper is the following: first of all in Section 2 we recall the basic equations of linear elastic problem, Section 3 we briefly recall the modified Hu-Washizu formulations as in B.P.Lamichhane et al. (2013), Section 4 we develop the novel finite element spaces adopted. Finally, Section 5 we report many examples to prove the efficiency of the studied element and Section 6 the final remarks and the future developments.

2. Linear elastic continuum problem

In this section we briefly recovery the equations governing the homogeneous isotropic linear elastic material body.

Let a bounded domain $\Omega \in \mathbb{R}^n$ with Lipschitz boundary $\Gamma = \Gamma_d \cup \Gamma_n$, where Γ_d and Γ_n are the Dirichlet and Neumann boundaries, respectively. The equilibrium equation is:

$$-\text{div}(\boldsymbol{\sigma}) = \mathbf{f} , \quad (1)$$

where $\boldsymbol{\sigma}$ is the Cauchy stress tensor and \mathbf{f} is the body forces per unit area or volume. The small strain tensor \mathbf{d} is defined by:

$$\mathbf{d} = \boldsymbol{\varepsilon}(\mathbf{u}) = \frac{1}{2}(\boldsymbol{\nabla} \mathbf{u} + \boldsymbol{\nabla} \mathbf{u}^T) , \quad (2)$$

where \mathbf{u} is the displacement field and $\boldsymbol{\nabla}$ is the gradient operator. In the case of linear elasticity we have:

$$\boldsymbol{\sigma} = \lambda \text{tr}(\boldsymbol{\varepsilon})\mathbf{I} + 2\mu \boldsymbol{\varepsilon} , \quad (3)$$

where μ and λ are the Lamé parameters depending by the material, $\text{tr}(\mathbf{a})$ is the trace of the tensor \mathbf{a} and \mathbf{I} is the identity tensor. Using the equation (3) and by some algebra one obtains:

$$\boldsymbol{\sigma} = \begin{pmatrix} \lambda(\varepsilon_{11} + \varepsilon_{22}) & 0 \\ 0 & \lambda(\varepsilon_{11} + \varepsilon_{22}) \end{pmatrix} + 2\mu \begin{pmatrix} \varepsilon_{11} & \varepsilon_{12} \\ \varepsilon_{12} & \varepsilon_{22} \end{pmatrix} , \quad (4)$$

and rearranging the equation (4):

$$\boldsymbol{\sigma} = \begin{pmatrix} (\lambda + 2\mu)\varepsilon_{11} + \lambda \varepsilon_{22} & 2\mu \varepsilon_{12} \\ 2\mu \varepsilon_{12} & (\lambda + 2\mu) \varepsilon_{22} + \lambda \varepsilon_{11} \end{pmatrix} . \quad (5)$$

Using the equations (1), (2) and (3) we obtain the resuming system for the linear elastic problem:

$$\begin{cases} \text{div}(\boldsymbol{\sigma}) + \mathbf{f} = \mathbf{0} , \\ \boldsymbol{\varepsilon}(\mathbf{u}) - \mathbf{d} = \mathbf{0} , \\ \boldsymbol{\sigma} - \mathbf{C}\mathbf{d} = \mathbf{0} , \end{cases} \quad (6)$$

where \mathbf{C} is the fourth order elastic tensor. On the boundary we have:

$$\begin{aligned} \mathbf{u}_d &= \bar{\mathbf{u}} , & \forall \mathbf{u} \subset \Gamma_d , \\ \mathbf{u}_n &= \mathbf{t} \cdot \mathbf{n} , & \forall \mathbf{u} \subset \Gamma_n , \end{aligned} \quad (7)$$

54 where \mathbf{t} are the distributed traction and \mathbf{n} is the unit normal vector along
 55 the Neumann boundary and $\bar{\mathbf{u}}$ is the prescribed displacement field along the
 56 Dirichlet boundary.

57 3. Briefly introduction to modify Hu-Washizu

58 Starting by the equations resumed in the system (6), need be tested with
 59 triplet of virtual displacements, strains, stresses, say $(\mathbf{v}, \mathbf{e}, \boldsymbol{\tau})$ to arrive at the
 60 classical Hu-Washizu variational principle reads:

$$\left\{ \begin{array}{ll} - \int_{\Omega} \boldsymbol{\sigma} : \boldsymbol{\varepsilon}(\mathbf{v}) + \int_{\Omega} \mathbf{f} \cdot \mathbf{v} = 0, & \forall \mathbf{v} \in V \\ \int_{\Omega} (\boldsymbol{\varepsilon}(\mathbf{u}) - \mathbf{d}) : \boldsymbol{\tau} = 0, & \forall \boldsymbol{\tau} \in S_0 \\ \int_{\Omega} \boldsymbol{\sigma} : \mathbf{e} - \int_{\Omega} \mathbf{C} \mathbf{d} : \mathbf{e} = 0, & \forall \mathbf{e} \in S \end{array} \right. \quad (8)$$

61 where we define the spaces $V = [H_0^1(\Omega)]^n$, $S = L^2(\Omega)_{sym}^{n \times n}$ and

$$S_0 = \left\{ \boldsymbol{\tau} \in S \mid \int_{\Omega} \boldsymbol{\tau} : \mathbf{I} = 0 \right\}. \quad (9)$$

62 The Hu-Washizu problem reads: Find $(\mathbf{u}, \mathbf{d}, \boldsymbol{\sigma}) \in V \times S \times S_0$ such that:

$$\left\{ \begin{array}{ll} \tilde{a}((\mathbf{u}, \mathbf{d}), (\mathbf{v}, \mathbf{e})) + b((\mathbf{v}, \mathbf{e}), \boldsymbol{\sigma}) = l(\mathbf{v}), & \forall (\mathbf{u}, \mathbf{d}) \in V \times S \\ b((\mathbf{u}, \mathbf{d}), \boldsymbol{\tau}) = 0, & \forall \boldsymbol{\tau} \in S_0 \end{array} \right. \quad (10)$$

63 Due to the lack of ellipticity of the bilinear form $\tilde{a}((\mathbf{u}, \mathbf{d}), (\mathbf{v}, \mathbf{e}))$ on the space
 64 $V \times S$, as you can see in B.P.Lamichhane et al. (2013) and B.P.Lamichhane
 65 (2009), a positive scalar α is introduced so as the replace the bilinear form
 66 from $\tilde{a}((\mathbf{u}, \mathbf{d}), (\mathbf{v}, \mathbf{e}))$ with

$$a((\mathbf{u}, \mathbf{d}), (\mathbf{v}, \mathbf{e})) = \int_{\Omega} \mathbf{d} : \mathbf{C} \mathbf{e} + \alpha \int_{\Omega} (\boldsymbol{\varepsilon}(\mathbf{u}) - \mathbf{d}) : (\boldsymbol{\varepsilon}(\mathbf{v}) - \mathbf{e}). \quad (11)$$

67 By so doing, one ends up with the following stable Hu-Washizu continuous
 68 formulation: Find $(\mathbf{u}, \mathbf{d}, \boldsymbol{\sigma}) \in V \times S \times S_0$ such that:

$$\left\{ \begin{array}{ll} a((\mathbf{u}, \mathbf{d}), (\mathbf{v}, \mathbf{e})) + b((\mathbf{v}, \mathbf{e}), \boldsymbol{\sigma}) = l(\mathbf{v}), & \forall (\mathbf{u}, \mathbf{d}) \in V \times S \\ b((\mathbf{u}, \mathbf{d}), \boldsymbol{\tau}) = 0, & \forall \boldsymbol{\tau} \in S_0 \end{array} \right. \quad (12)$$

69 4. Finite element discretization

70 We consider a quasi-uniform triangulation \mathcal{T}_h of the polygonal domain
 71 Ω consists of simply, either quadrilateral or hexahedral. We take into ac-
 72 count of standard bilinear finite element space $K_h \subset H^1(\Omega)$ defined on the
 73 triangulation \mathcal{T}_h , where:

$$K_h := \{v \in C^0(\Omega) : v|_T \in \mathcal{Q}_1(T), T \in \mathcal{T}_h\}, \quad K_h^0 = K_h \cap H_0^1(\Omega), \quad (13)$$

74 and the space of bubble functions

$$B_h := \left\{ b_T \in H^1(T) : b_{T|\partial T} = 0 \text{ and } \int_T b_T dx > 0, T \in \mathcal{T}_h \right\}, \quad (14)$$

75 and we define the spaces for strain and displacement as $\mathbf{S}_h := [K_h]^{2 \times 2}$ and
 76 $\mathbf{V}_h := [K_h^0 \oplus B_h]^2$. In the next section we discuss the different choosing of
 77 bubble functions. For the discrete stress space we use:

$$\mathbf{M}_h := \left\{ \boldsymbol{\tau}_h \in [M_h]^{2 \times 2} : \int_{\Omega} \boldsymbol{\tau}_h : \mathbf{1} dx = 0 \right\} \subset \mathbf{S}_0, \quad (15)$$

78 and let $\{\phi_1, \dots, \phi_n\}$ and $\{\mu_1, \dots, \mu_n\}$ the n the basis functions for the space
 79 V_h and M_h respectively, we construct the functions μ_i using the following
 80 biorthogonality property between the space V_h and M_h :

$$\int_{\Omega} \mu_i \phi_j dx = c_j \delta_{ij}, \quad c_j \neq 0, \quad 1 \leq i, j \leq n, \quad (16)$$

81 where δ_{ij} is Kronecker symbol, and c_j is a scaling factor which can be
 82 chosen to be proportion al to the area of support of ϕ_j . The local ba-
 83 sis function of K_h and M_h for the reference square element (see figure 1)
 84 $\hat{T} := \{(\xi, \eta) : -1 \leq \xi \leq 1, -1 \leq \eta \leq 1\}$ are:

$$\begin{aligned} \hat{\phi}_1 &= \frac{1}{4}(1 - \xi)(1 - \eta), & \hat{\phi}_2 &= \frac{1}{4}(1 + \xi)(1 - \eta), \\ \hat{\phi}_3 &= \frac{1}{4}(1 + \xi)(1 + \eta), & \hat{\phi}_4 &= \frac{1}{4}(1 - \xi)(1 + \eta). \end{aligned} \quad (17)$$

85 and

$$\begin{aligned} \hat{\mu}_1 &= 1 - 3\xi - 3\eta + 9\xi\eta, & \hat{\mu}_2 &= 1 + 3\xi - 3\eta - 9\xi\eta, \\ \hat{\mu}_3 &= 1 + 3\xi + 3\eta + 9\xi\eta, & \hat{\mu}_4 &= 1 - 3\xi + 3\eta + 9\xi\eta. \end{aligned} \quad (18)$$

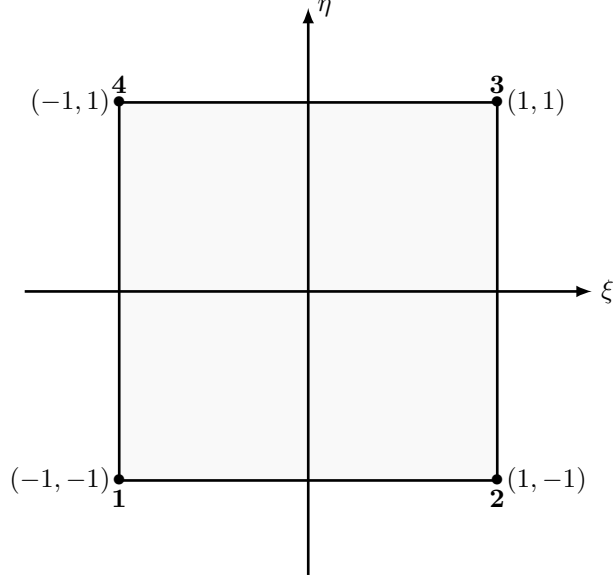


Figure 1: Reference Element

86 It is important to observe that the global basis functions of the space M_h are
 87 not continuous.

88 Now it is possible to write the weak discrete problem as: Find $(\mathbf{u}_h, \mathbf{d}_h, \boldsymbol{\sigma}_h) \in$
 89 $V_h \times S_h \times M_h$ such that:

$$\begin{cases} a((\mathbf{u}_h, \mathbf{d}_h), (\mathbf{v}_h, \mathbf{e}_h)) + b((\mathbf{v}_h, \mathbf{e}_h), \boldsymbol{\sigma}_h) = l(\mathbf{v}_h), & \forall (\mathbf{u}_h, \mathbf{d}_h) \in V_h \times S_h \\ b((\mathbf{u}_h, \mathbf{d}_h), \boldsymbol{\tau}_h) = 0, & \forall \boldsymbol{\tau}_h \in M_h \end{cases} \quad (19)$$

90 The matrix-vector form of the weak variational system (19) may then be
 91 written as

$$\begin{bmatrix} \alpha \mathbf{A} & -\alpha \mathbf{B} & \mathbf{W} \\ -\alpha \mathbf{B}^T & \mathbf{K} + \alpha \mathbf{M} & -\mathbf{D} \\ \mathbf{W}^T & -\mathbf{D}^T & \mathbf{0} \end{bmatrix} \begin{bmatrix} \mathbf{x}_u \\ \mathbf{x}_d \\ \mathbf{x}_\sigma \end{bmatrix} = \begin{bmatrix} \mathbf{b}_f \\ \mathbf{0} \\ \mathbf{0} \end{bmatrix}, \quad (20)$$

92 where

$$\begin{aligned}
\mathbf{A} &= \int_{\Omega} \boldsymbol{\varepsilon}(\mathbf{u}_h) : \boldsymbol{\varepsilon}(\mathbf{v}_h) , & \mathbf{B} &= \int_{\Omega} \mathbf{d}_h : \boldsymbol{\varepsilon}(\mathbf{v}_h) , \\
\mathbf{W} &= \int_{\Omega} \boldsymbol{\sigma}_h : \boldsymbol{\varepsilon}(\mathbf{v}_h) , & \mathbf{K} &= \int_{\Omega} \mathbf{C} \mathbf{e}_h : \mathbf{d}_h , \\
\mathbf{M} &= \int_{\Omega} \mathbf{e}_h : \mathbf{d}_h , & \mathbf{D} &= \int_{\Omega} \boldsymbol{\sigma}_h : \mathbf{e}_h .
\end{aligned} \tag{21}$$

93 \mathbf{D} is a diagonal matrix. Using the property in equation (16) it is possible to
94 condense statically \mathbf{x}_d and \mathbf{x}_σ , and we obtain the following system in only
95 displacement unknown \mathbf{x}_u :

$$[\alpha \mathbf{A} - \alpha (\mathbf{B} \mathbf{D}^{-1} \mathbf{W}^{-T} + \mathbf{W} \mathbf{D}^{-1} \mathbf{B}^T) + \mathbf{W} \mathbf{D}^{-1} (\mathbf{K} + \alpha \mathbf{M}) \mathbf{D}^{-1} \mathbf{W}^T] \mathbf{x}_u = \mathbf{b}_f, \tag{22}$$

96 whereas strains and stresses may be evaluated afterwards by back-substitution.

97 4.1. Bubble functions

98 In this section we detail the different choosing of the bubble functions.
99 Addition of the bubble functions is essential to create a stable space. Ac-
100 cordingly to W.Bai (1997) and B.P.Lamichhane (2015), we obtain four
101 types of elements with different bubble functions. In the first two cases we
102 use a modification of the standard bubble function ,that is for the reference
103 element:

$$\hat{b}_T(\xi, \eta) = (1 - \xi^2)(1 - \eta^2) , \tag{23}$$

104 while in the next two, we add to the standard bubble function another one.

105 4.1.1. One Bubble function (type 1)

106 As a first choice of bubble function we use:

$$\hat{b}_{T,1}(\xi, \eta) = c_T \cdot \phi_T(\xi, \eta) \cdot \hat{b}_T(\xi, \eta) , \tag{24}$$

107 where c_T is a coefficient in order to obtain $\hat{b}_{T,1}(\xi_g, \eta_g) = 1$ (where \mathbf{g} is the
108 centroid of the elements), ϕ_K is the standard bilinear basis function corre-
109 sponding to the lower-left corner of the square T . In the case of reference
110 square element we obtain:

$$\hat{b}_{T,1}(\xi, \eta) = (1 - \xi)(1 - \eta)(1 - \xi^2)(1 - \eta^2) . \tag{25}$$

111 *4.1.2. One Bubble function (type 2)*

112 The second choice of bubble function we take:

$$\hat{b}_{T,1}(\xi, \eta) = c_T \cdot (a + b\xi + c\eta) \cdot \hat{b}_T(\xi, \eta) , \quad (26)$$

113 where $a, b, c \in \mathbb{R}$ and $a, b, c \neq 0$. For simplicity we should take $a = b = c = 1$
 114 and we obtain for the reference square:

$$\hat{b}_{T,1}(\xi, \eta) = (1 + \xi + \eta)(1 - \xi^2)(1 - \eta^2) . \quad (27)$$

115 *4.1.3. Two Bubble functions*

116 Using two bubble functions, where the first is the standard bubble func-
 117 tion and the second bubble is a modification of the standard bubble. We
 118 define a new space of bubble functions as follow:

$$\hat{B}_h^+ = \left\{ \hat{\mathbf{v}} \in B_h \mid \hat{\mathbf{v}} = [\mathbf{v}_0 + \mathbf{v}_{01}(a\xi + b\eta)] \hat{b}_T, \mathbf{v}_0, \mathbf{v}_{01} \in \mathbb{R}^2 \right\} , \quad (28)$$

119 where a and b are two arbitrary constants satisfying $a^2 + b^2 \neq 0$. For the
 120 sake of simplicity should take $a = b = 1$. The two bubble functions are:

$$\begin{aligned} \hat{b}_{T,1}(\xi, \eta) &= \hat{b}_T , \\ \hat{b}_{T,2}(\xi, \eta) &= (\xi + \eta) \hat{b}_T . \end{aligned} \quad (29)$$

121 *4.1.4. Two Bubble functions, which one mixed*

122 As a finally choice of bubbles we use a standard bubble function plus one
 123 mixed bubble function for the two components of displacement. We define
 124 the modify space of bubble functions:

$$\hat{B}_h^{++} = \left\{ \hat{\mathbf{v}} \in B_h \mid \hat{\mathbf{v}} = \left[\mathbf{v}_0 + w_0 \nabla \hat{\phi}_1 \right] \hat{b}_T, \mathbf{v}_0 \in \mathbb{R}^2, w_0 \in \mathbb{R} \right\} , \quad (30)$$

125 where $\nabla \hat{\phi}_1$ is the gradient of the first shape function $\hat{\phi}$. The two bubble
 126 functions are:

$$\begin{aligned} \hat{b}_{T,1}(\xi, \eta) &= \hat{b}_T , \\ \hat{\mathbf{b}}_{T,2}(\xi, \eta) &= \left[\hat{\phi}_{1,\xi}, \hat{\phi}_{1,\eta} \right] \hat{b}_T , \end{aligned} \quad (31)$$

127 where $\hat{\phi}_{1,\xi}, \hat{\phi}_{1,\eta}$ are the derivatives of the first shape function $\hat{\phi}$ to ξ and η
 128 respectively. We can observe that $\hat{\mathbf{b}}_{T,2}$ is a vector.

129 5. Numerical examples

130 In this section we report some examples using the presented formulation
 131 to proven the good behaviour. All examples are studied in nearly incom-
 132 pressible limit.

133 5.1. Square problem

134 First example is a unit square domain with homogeneous Dirichlet bound-
 135 ary conditions. This benchmark problem is analyzed in S.C. Brenner (1993).
 136 The Lamé constant are fix to $\nu = 0.49995$ and $\mu = 1$. We impose the follow-
 137 ing body forces:

$$\begin{aligned} f_1 &= \beta \left(\pi^2 (4 \sin(\pi y) (-1 + 2 \cos(2\pi x)) - \cos(\pi(x+y)) \right. \\ &\quad \left. + A \sin(\pi x) \sin(\pi y)) \right) , \\ f_2 &= \beta \left(\pi^2 (4 \sin(2\pi x) (1 - 2 \cos(2\pi y)) - \cos(\pi(x+y)) \right. \\ &\quad \left. + A \sin(\pi x) \sin(\pi y)) \right) , \end{aligned} \quad (32)$$

138 where

$$A = \frac{2}{1 + \lambda} \text{ and } \beta = \frac{1}{25} . \quad (33)$$

139 By imposition of the previously body forces the exact solution is:

$$\begin{aligned} u_1 &= \beta (\sin(2\pi y) (-1 + \cos(2\pi x)) + B) , \\ u_2 &= \beta (\sin(2\pi x) (1 - \cos(2\pi y)) + B) , \end{aligned} \quad (34)$$

140 where

$$B = 0.5A \sin(\pi x) \sin(\pi y) . \quad (35)$$

141 The problem is studied using two type of mesh: first of all using a square
 142 mesh and before using a trapezoidal mesh. The two types of mesh are shown
 143 in figures 2(a) and 2(b). Figures 3(a), 3(b), 4(a) and 4(b) shown the error
 144 in norm L^2 in the case of regular mesh for the different types of bubble
 145 functions and coefficients α . All types of element converge in a good way. In
 146 Figures 5(a), 5(b), 6(a) and 6(b) we report the previously results in the case
 147 of trapezoidal meshes. In this example do not see an appreciable difference
 148 between the different choices of the α coefficient and types of mesh.

149 In figures 7(a), 7(b), 8(a), 8(b), 9(a), 9(b), 10(a) and 10(b) we report
 150 the error in L^2 norm of the strain d_{xx} for the the different choice of bubble
 151 functions and coefficient α .

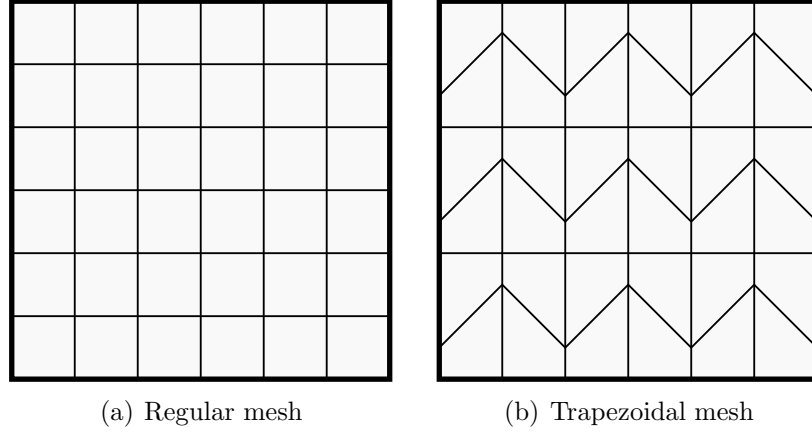


Figure 2: Square Problem

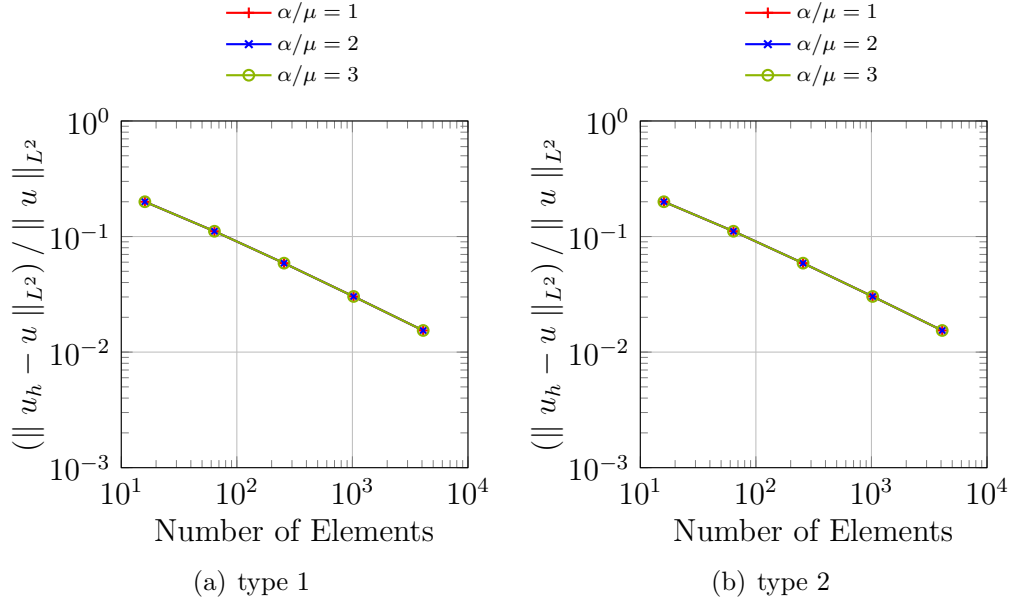


Figure 3: The relative error vs. the number of elements measured relative to the L^2 norm (Case one bubble function and regular mesh)

152 5.2. Cantilever beam problem

153 Now we consider the beam with length $L = 10$ and height $l = 2$ as
 154 we shown in figure 11. The Young modulus is set equal to $E = 1500$ and

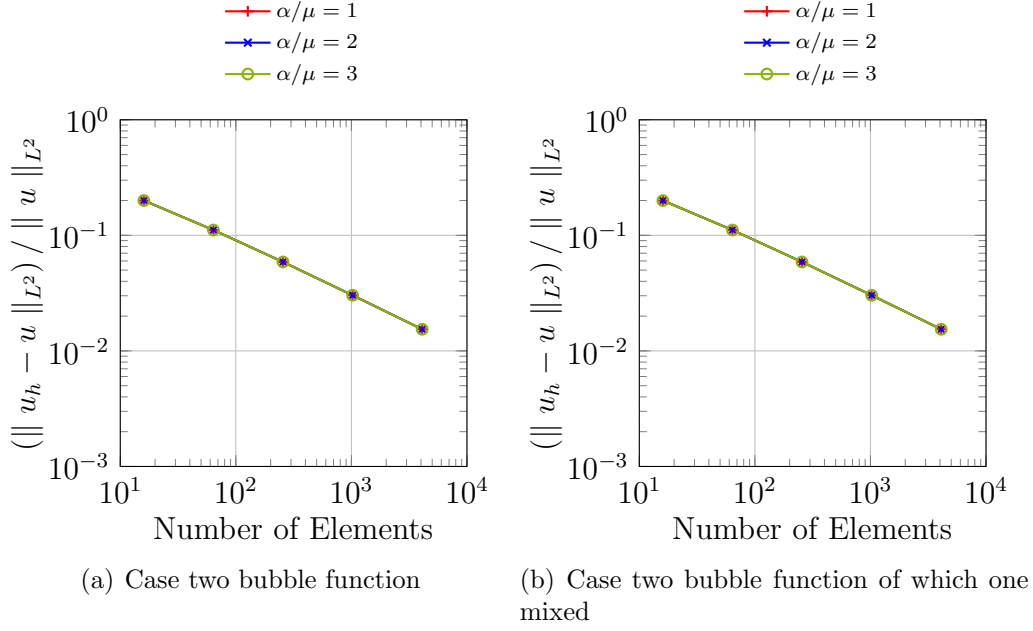


Figure 4: The relative error versus the number of elements measured relative to the L^2 norm (regular mesh)

the Poisson $\nu = 0.4999$. The beam are fixed in the bottom left corner and subjected to a distributed load with $f = 300$ on the right edge as shown in figure 11. The exact solution reported in J.K.Djoko and B.D.Reddy (2006) is:

$$\begin{aligned} u(x, y) &= \frac{2f}{El}(1 - \nu^2)x \left(\frac{l}{2} - y \right), \\ v(x, y) &= \frac{f}{El} \left[x^2 + \frac{\nu}{1 - \nu} (y^2 - ly) \right]. \end{aligned} \quad (36)$$

We use to model the beam two types of mesh: regular and trapezoidal as in the previously example (see figures 2(a) and 2(b)).

In figure 12 is shown the deformation resulting using 2000 elements with two bubble functions while in figure 13 and 14 are shown the comparison between the computed strain component $[\mathbf{d}_h]_{xx}$ and $[\mathbf{d}_h]_{yy}$ and the analytic strain component $[\mathbf{d}]_{xx}$ and $[\mathbf{d}]_{yy}$. The computed strain components are in a good agreement with the analytical ones.

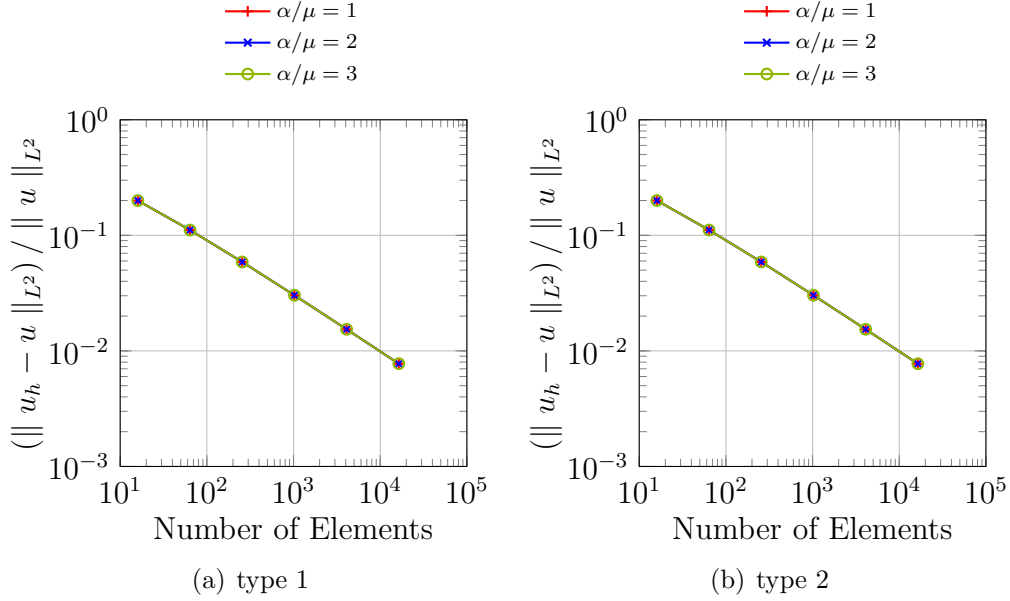


Figure 5: The relative error vs. the number of elements measured relative to the L^2 norm (Case one bubble function and Trapezoidal mesh)

166 In figures 17(a), 17(b), 18(a) and 18(b) are shown the L^2 -norm error for
 167 different types of bubble functions used in the case of $\alpha/\mu := 1, 2, 3$, while
 168 in figures 17(a), 17(b), 18(a) and 18(b) the same plots using trapezoidal
 169 meshes. In all examples the parameter α influences the magnitude of the
 170 relative error but not the rate of convergence. Furthermore the distorted
 171 elements have a negligible difference in comparison to the regular mesh.

172 5.3. Cook's membrane

173 The final example is the Cook's membrane. That is a typical benchmark
 174 and consist of a beam with vertex: $(0, 0)$, $(48, 44)$, $(48, 60)$ and $(0, 44)$. The
 175 left vertical edge is clamped and the right vertical edge subjected to the
 176 vertical distributed forces with resultant $F = 100$ as it shown in figure 19.
 177 The material properties are taken to be $E = 250$ and $\nu = 0.4999$, so that a
 178 nearly incompressible response is obtained. We report in figures 20(a), 20(b),
 179 20(c) and 20(d) the vertical displacement of the point A versus the number
 180 of element per side for different choices of the parameter $\alpha = \{1, \mu, 2\mu, 3\mu\}$.
 181 The parameter α greatly influence the results, indeed, in the case of $\alpha = 1$,

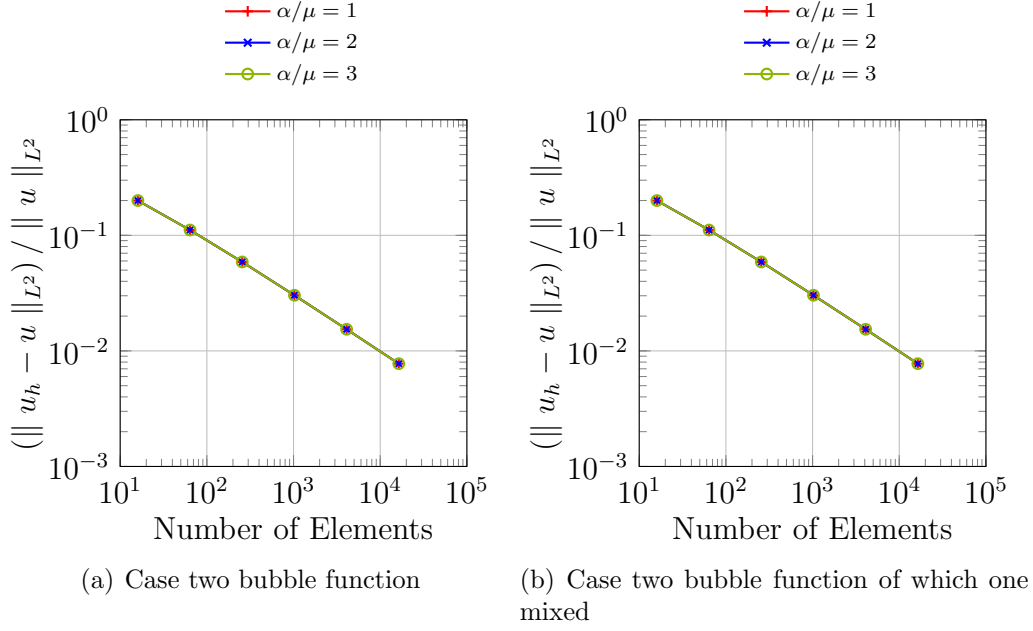


Figure 6: The relative error vs. the number of elements measured relative to the L^2 norm (Case one bubble function and Trapezoidal mesh)

182 figure 20(a), the obtained results are completely incorrect. However, the
 183 convergence is archived for all elements in the case of the normal range of
 184 the parameter α . No locking phenomenon is highlighted in any of the cases.

185 6. Conclusions

186 We present a new family of quadrilaterals mixed finite elements based
 187 on a modified Hu-Washizu formulation. Different types of enrichment of
 188 the displacement field were successfully tested in the case of incompressible
 189 regime and trapezoidal meshes.

190 The future developments are oriented to finding an optimal choosing of
 191 the parameter α and the extension to the 3-D case using hexahedral elements.

192 W.Bai. "The quadrilateral 'Mini' finite element for Stokes problem", *Comput.*
 193 *Methods Appl. Mech. Engrg.*, 143: 41-47, 1997.

194 D.Boffi. "On the finite element method on quadrilateral meshes", *Appl. Num.*
 195 *Mathematics*, 56: 1271-1282, 2006.

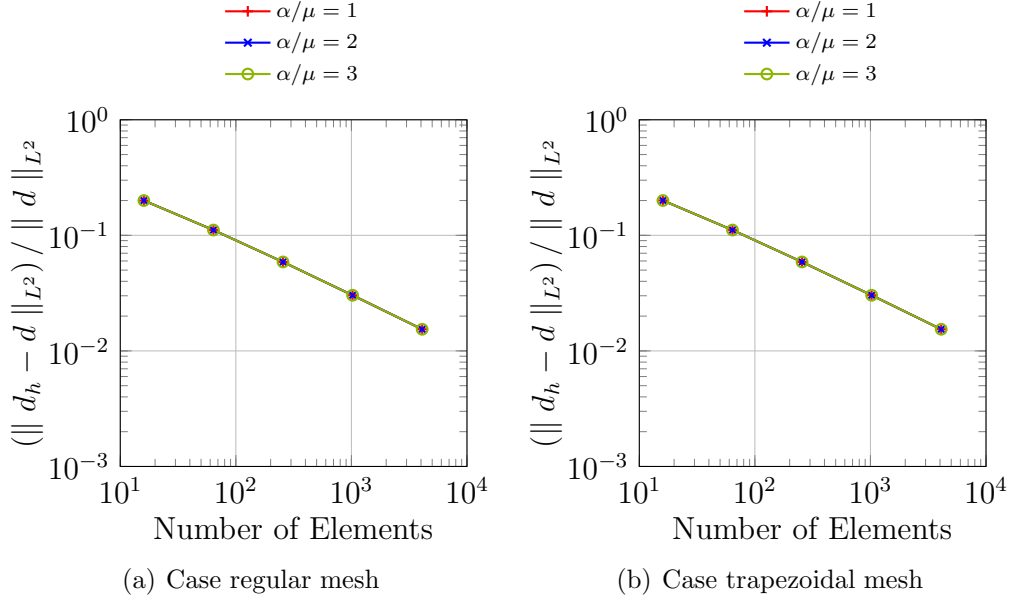


Figure 7: The relative error of strain \mathbf{d}_{xx} vs. the number of elements (Case of two bubble functions)

- 196 B.P.Lamichhane. “A quadrilateral ‘mini’ finite element for the Stokes prob-
 197 lem using a single bubble function”, *Appl. Num. Math.*, 56: 1271-1282,
 198 2015.
- 199 J.K.Djoko, B.D.Reddy. “An extended Hu-Washizu formulation for elastic-
 200 ity”, *Comput. Methods Appl. Mech. Engrg.*, 195: 6330-6346, 2006.
- 201 B.P.Lamichhane, A.T.McBride, B.D.Reddy. “A finite element method for
 202 three-field formulation of linear elasticity based on biorthogonal systems”,
 203 *Comput. Methods Appl. Mech. Engrg.*, 258: 109-117, 2013.
- 204 B.P.Lamichhane, B.D.Reddy, B.I.Wohlmuth. “Convergence in the incom-
 205 pressible limit of finite element approximation based on Hu-Washizu for-
 206 mulation”, *Numer. Math.*, 104: 151-175, 2006.
- 207 D.Boffi, C.Lovadina. “Analisy of new augmented Lagrangian formulation
 208 for mixed finite element schemes”, *Numer. Math.*, 75: 405-419, 1997.

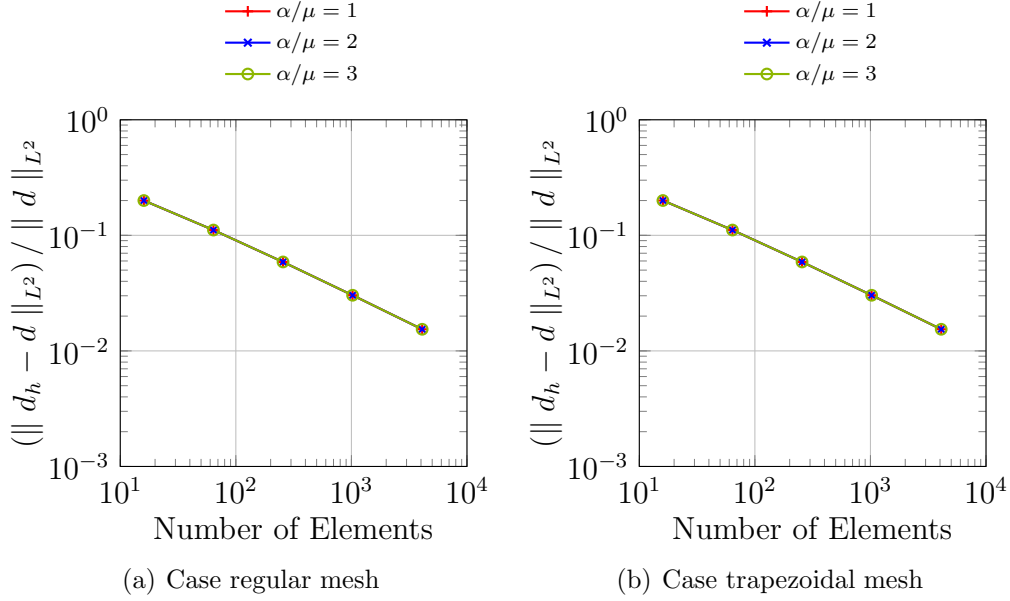


Figure 8: The relative error of strain \mathbf{d}_{xx} vs. the number of elements (Case of two bubble functions, which one mixed)

- 209 B.P.Lamichhane. “From the Hu-Washizu formulation to the average nodal
210 strain formulation”, *Comput. Methods Appl. Mech. Engrg.*, 198: 3957-3961,
211 2009.
- 212 D.N.Arnold, R.Winther. “Mixed finite elements for elasticity”, *Numer.*
213 *Math.*, 92: 401-419, 2002.
- 214 D.Boffi, F.Brezzi, M.Fortin. “Mixed Finite Element Methods and Applica-
215 tions”, *Springer Series in Computational Mathematics*, Vol.44, 2013.
- 216 D.N.Arnold, G.Awanou. “Rectangular mixed finite elements for elasticity”,
217 *Models Methods Appl. Sci.*, 15: 1417-1429, 2005.
- 218 H.Hu. “On some variational principles in the theory of elasticity and the
219 theory of plasticity”, *Sci. Sin.*, 4: 33-54, 1955.
- 220 K.Washizu. “Variational Methods in Elasticity and Plasticity, third ed.”,
221 *Pergamon Press*, 1982.

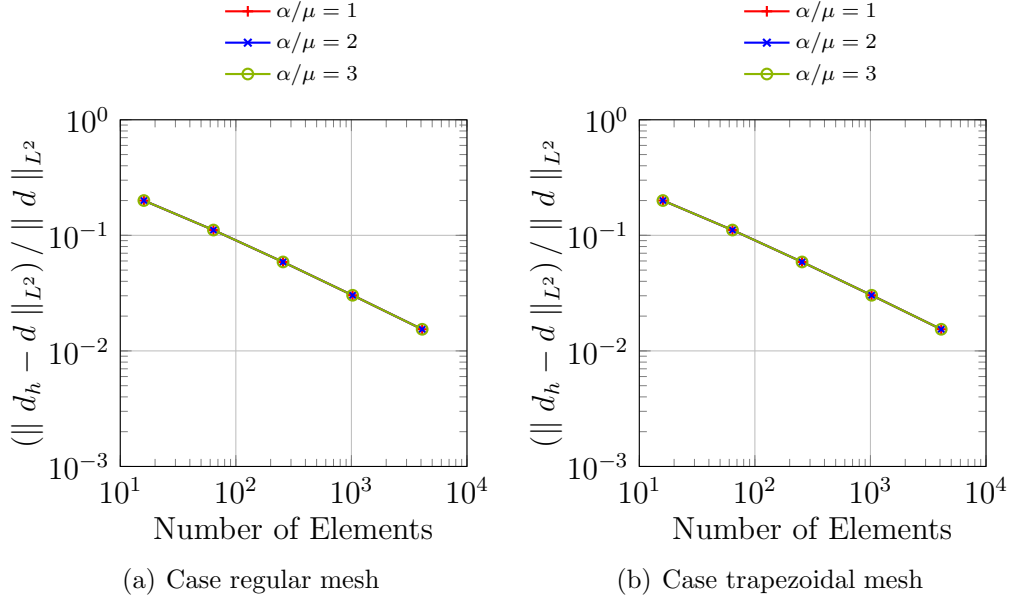


Figure 9: The relative error of strain \mathbf{d}_{xx} vs. the number of elements (Case of one bubble function type 1)

- 222 B.M. Fraeijis de Veubeke. “Diffusion des inconnues hyperstatiques dans les
 223 voilures á longeron couplés”, *Bull. Serv. Technique de l’Aeronautique Im-*
 224 *premérie Marcel Hayez*, Bruxelles, 1951.
- 225 E.P. Kasper, R.L. Taylor. “A mixed-enhanced strain method Part I: geomet-
 226 rically linear problems”, *Comput. Struct.*, 75: 237-250, 2000.
- 227 E.P. Kasper, R.L. Taylor. “A mixed-enhanced strain method Part II: geo-
 228 metrically nonlinear problems”, *Comput. Struct.*, 75: 251-260, 2000.
- 229 S.C. Brenner. “A nonconforming mixed multigrid method for the pure dis-
 230 placement problem in planar linear elasticity”, *SIAM J. Numer. Anal.*, 30:
 231 116–135, 1993.

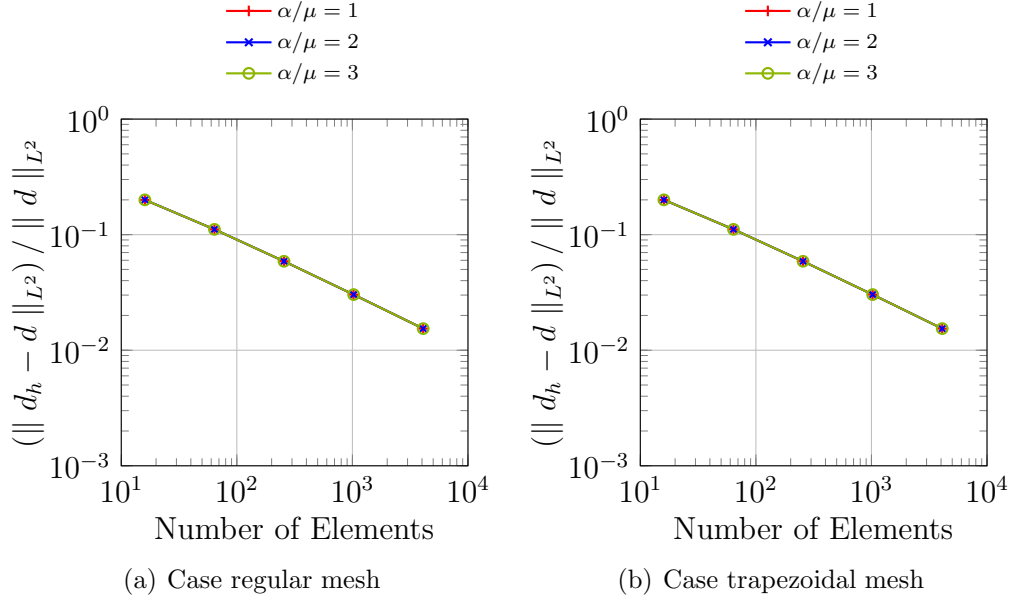


Figure 10: The relative error of strain d_{xx} vs. the number of elements (Case of one bubble function type 2)

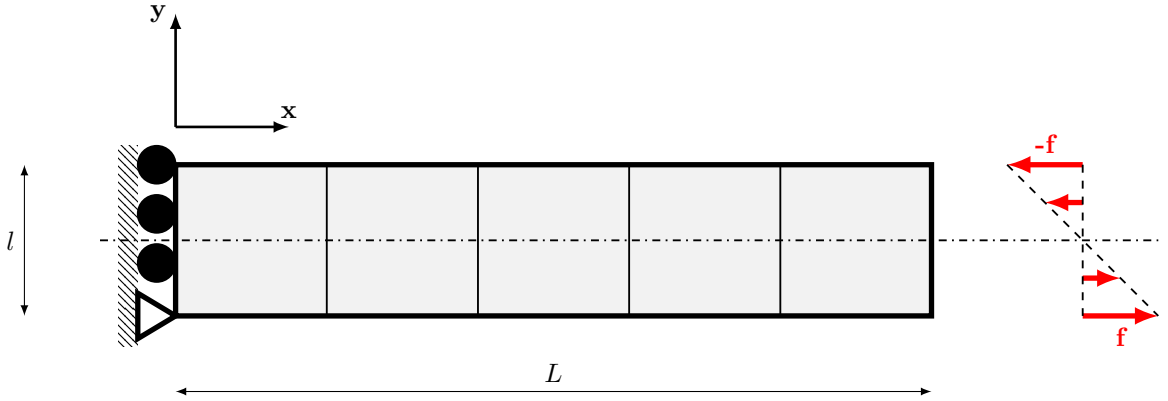


Figure 11: Beam cantilever geometry

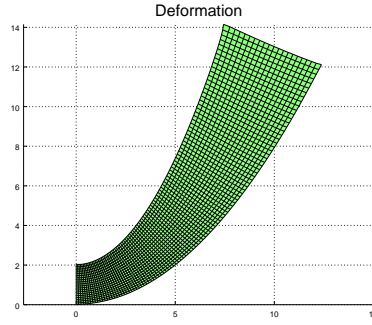


Figure 12: Beam Cantilever: deformation plot using 2000 elements with two bubble functions and $\alpha/\mu = 1$

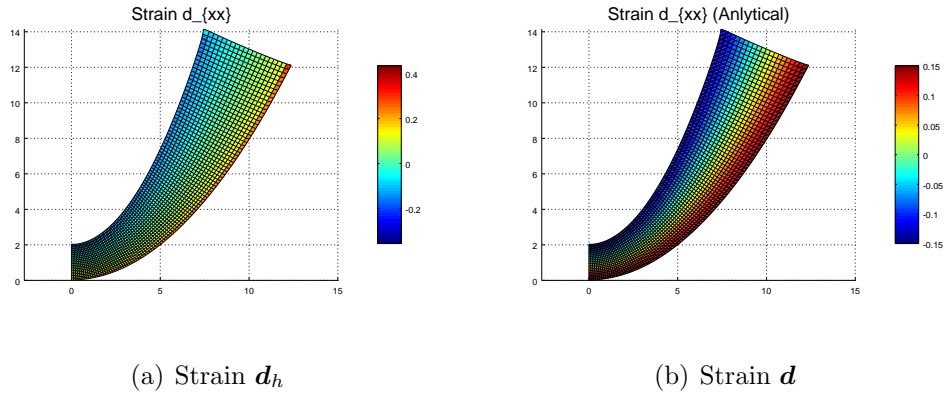
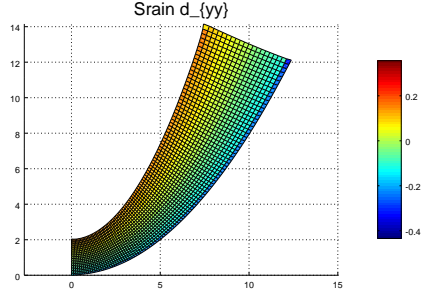
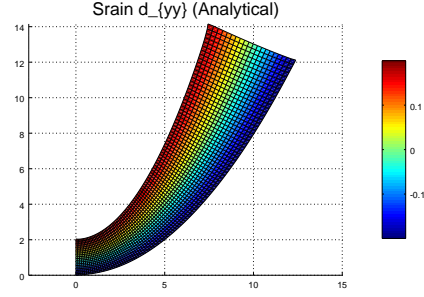


Figure 13: Beam Cantilever: strain $[\mathbf{d}_h]_{xx}$ vs. $[\mathbf{d}]_{xx}$ using 2000 elements with two bubble functions and $\alpha/\mu = 1$

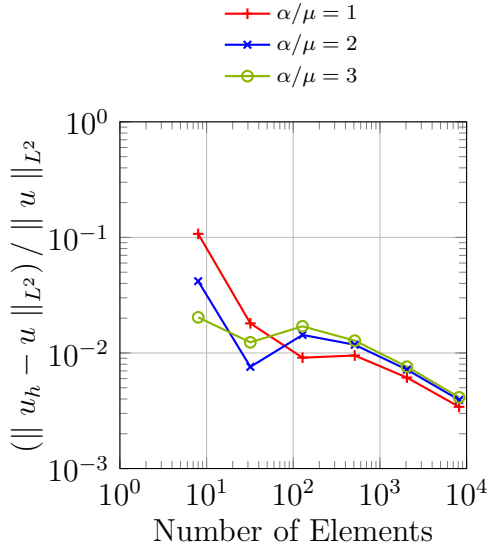


(a) Strain \mathbf{d}_h

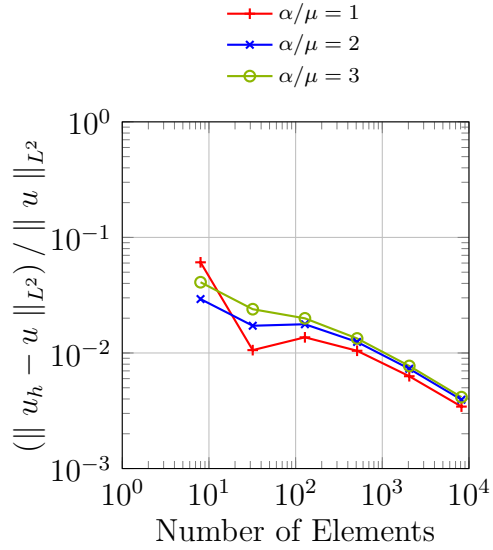


(b) Strain \mathbf{d}

Figure 14: Beam Cantilever: strain $[\mathbf{d}_h]_{yy}$ vs. $[\mathbf{d}]_{yy}$ using 2000 elements with two bubble functions and $\alpha/\mu = 1$

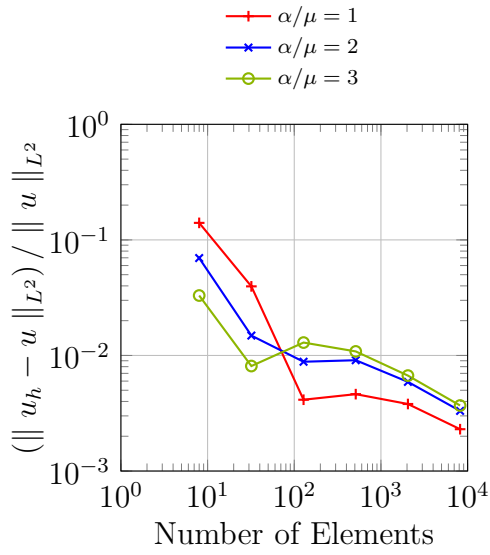


(a) Type 1

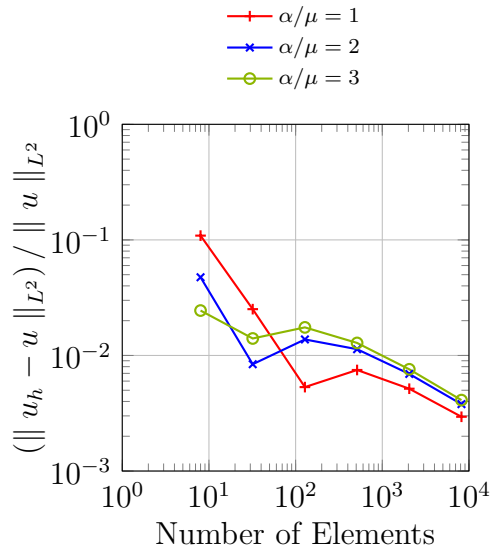


(b) Type 2

Figure 15: Beam Cantilever: the relative error vs. the number of elements measured relative to the L^2 norm (regular mesh)



(a) Case two bubble function



(b) Case two bubble function of which one mixed

Figure 16: Beam Cantilever: the relative error vs. the number of elements measured relative to the L^2 norm (regular mesh)

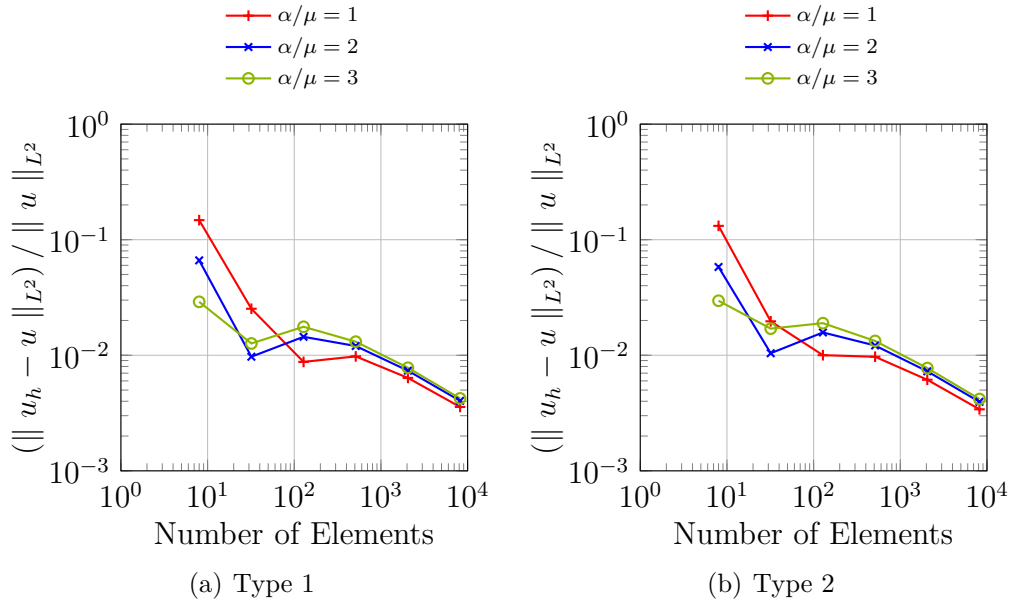


Figure 17: Beam Cantilever: the relative error vs. the number of elements measured relative to the L^2 norm (trapezoidal mesh)

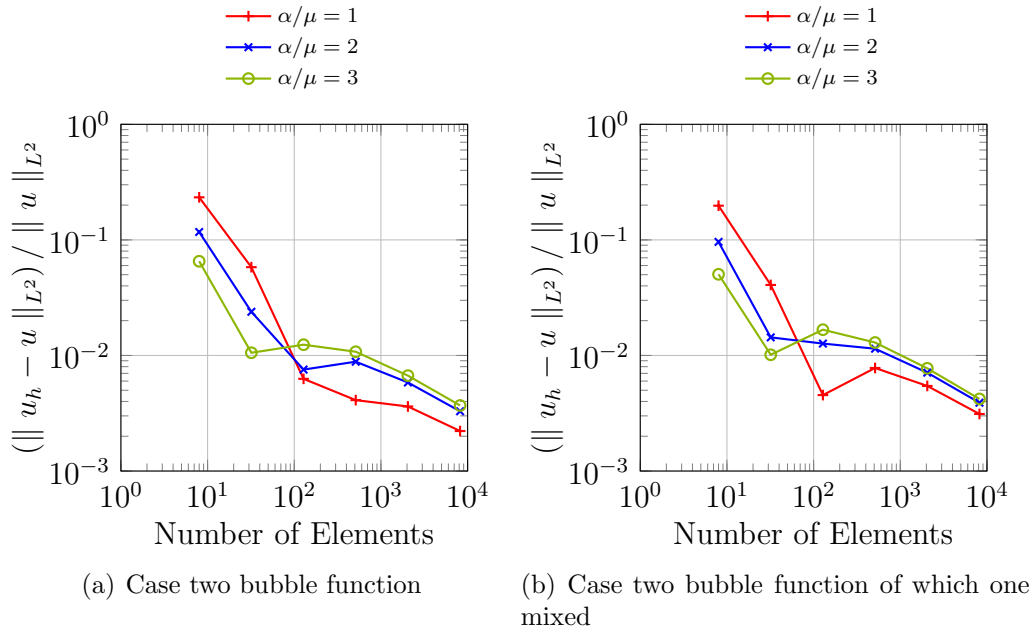


Figure 18: Beam Cantilever: the relative error vs. the number of elements measured relative to the L^2 norm (trapezoidal mesh)

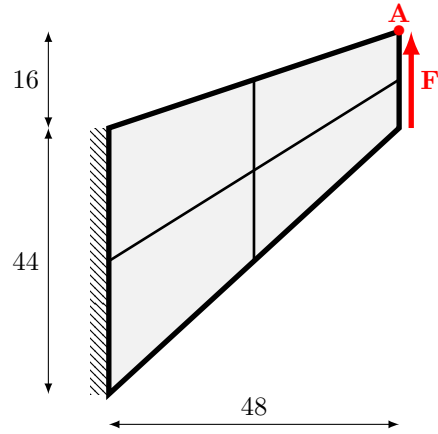


Figure 19: Cook's Membrane geometry

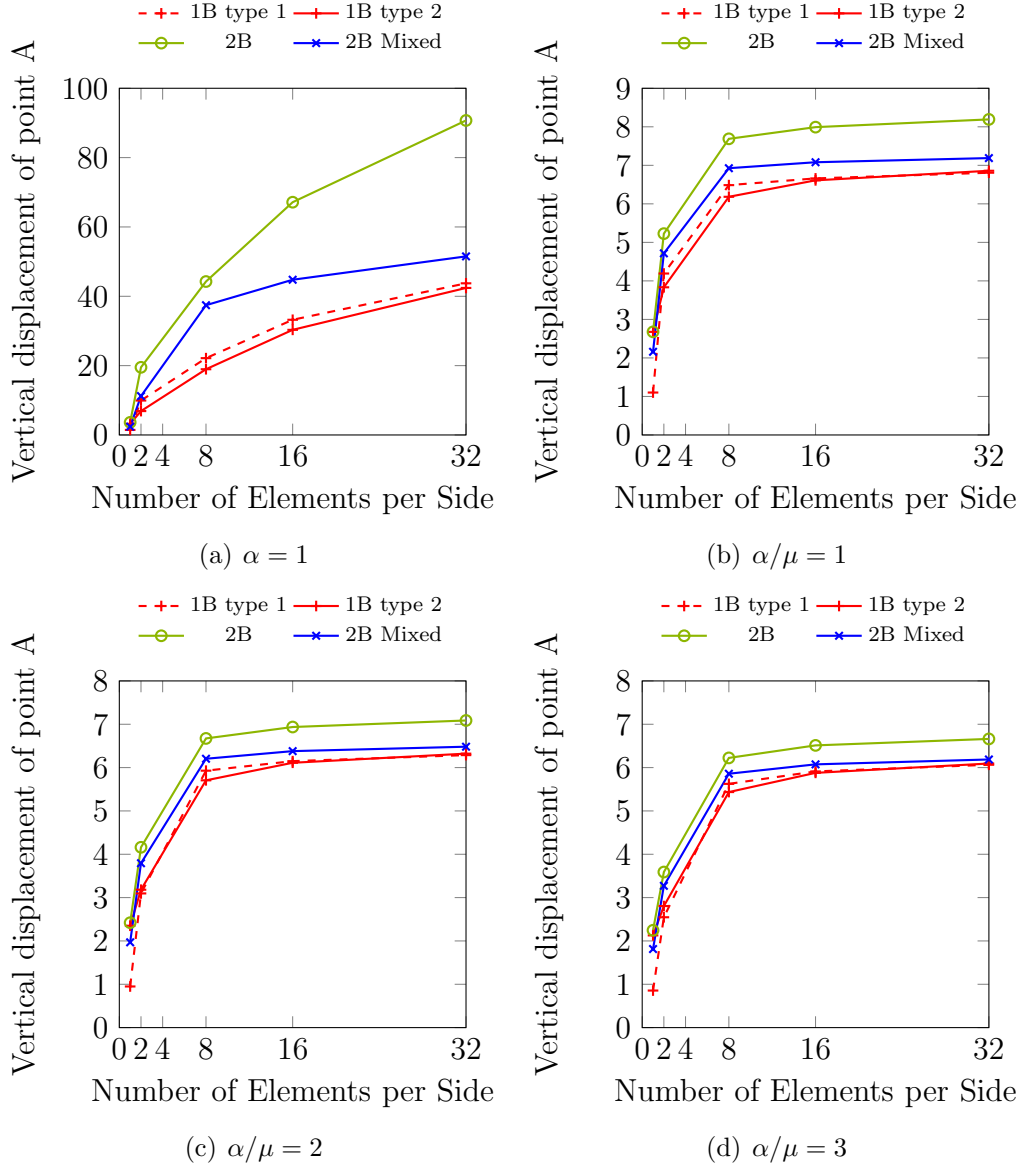


Figure 20: Vertical Displacement of point A vs. the number of elements per side